Inorganic Chemistry

Article

pubs.acs.org/IC

Structural Phase Transitions on AgCuS Stromeyerite Mineral under Compression

D. Santamaria-Perez,*[,†,‡] A. Morales-Garcia,[†,‡] D. Martinez-Garcia,[§,‡] B. Garcia-Domene,[§,‡] C. Mühle,[⊥] and M. Jansen[⊥]

[†]Departamento de Química-Física I, Universidad Complutense de Madrid, Avenida Complutense s/n, 28040 Madrid, Spain

[§]Departamento de Física Aplicada-ICMUV, Universidad de Valencia, Edificio de Investigación, C/Dr. Moliner 50, 46100 Burjassot, Valencia, Spain

[⊥]Max-Planck Institut für Festkörperforschung, Heisenbergstrasse 1, 70569 Stuttgart, Germany

ABSTRACT: The structural behavior of mineral Stromeyerite, AgCuS, has been studied by means of angle-dispersive X-ray diffraction measurements up to 13 GPa and ab initio total-energy calculations. Two high-pressure phase transitions are found at 1.4 and 5.7 GPa, from the initial distorted Ni_2In-type phase (AuRbS-type, RP, space group $Cmc2_1$) through an anti-PbClF-type phase (HP1, space group $P4/nmm$) to a monoclinic distortion of this latter phase (HP2, space group $P2_1/m$). The collapse of the metal−metal interatomic distances at the RP−HP1 transition suggests a stronger metallic behavior of the high-pressure phase. The compressibility of the lattice parameters and the equation of state of the first pressure-induced phase have been experimentally determined. First-principles calculations present an overall agreement with the experimental results in terms of the high-pressure sequence and provide chemical insight into the AgCuS behavior under hydrostatic pressure.

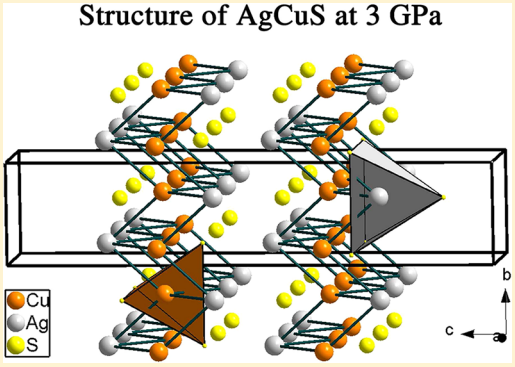

1. INTRODUCTION

Stromeyerite has long been recognized as a distinct mineral that usually occurs in nature in copper and silver ores. Its name comes from the german chemist Stromeyer, who, in 1816, was the first to analyze it. However, the exact composition of this mineral was first deduced by Guild in 1917 and defined as composed of a 1:1 ratio of the silver and cuprous sulfides.[1] In other words, it was a definite compound with the formula AgCuS. More recently, Schwartz[2] and Suhr[3] observed that when stromeyerite samples were prepared synthetically from either the proper powdered Cu_2S and Ag_2S proportions or the proper elemental proportions, silver metal and/or jalpaite (a silver-rich copper sulfide, Ag_3CuS_2) existed as additional phases. This experimental evidence suggest that stromeyerite could be slightly deficient in silver content and that a more accurate formula would be $Ag_{1-x}CuS$, where x ranges between 0 and 0.1.[4]

At room conditions, silver−copper sulfide AgCuS can be described with an orthorhombic space group $Cmc2_1$ (No. 36), as deduced by convergent-beam electron diffraction.[5] Its structure is based on a distorted hexagonal close packing (hcp) of S atoms. The Cu atoms, which lie in the hcp S layers, are three-coordinated, whereas the Ag atoms form loosely packed face-centered-cubic (fcc) layers that alternate with those of CuS and are bonded to two S atoms with a near-linear geometry[4,5] (see Figure 1). In addition to this phase, hereafter denoted as β, several others have been observed at different temperatures. Thus, the following phase transitions occur in

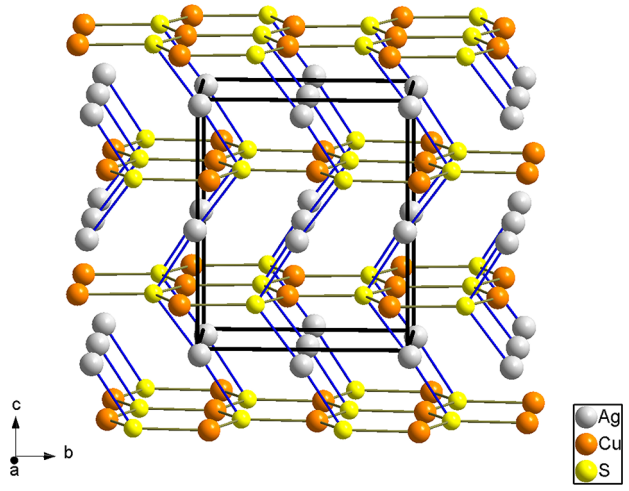

Figure 1. Structure of AgCuS at room conditions.

AgCuS: $\gamma \xrightarrow{120\ K} \beta \xrightarrow{361\ K} \alpha \xrightarrow{439\ K} \delta$. The γ polymorph, which is described in the *klassengleiche* subgroup $Pmc2_1$ (No. 26),[5] is just a slight distortion of the room-temperature structure. The high-temperature (HT) phases α and δ are described with hexagonal $P6_3/mmc$ and cubic $Fm\bar{3}m$ space groups, respectively.[6−8] In the

Received: September 28, 2012
Published: December 17, 2012

first HT α phase, the S atoms still adopt an hcp structure, with the Ag and Cu atoms partially disordered.[8] The second HT δ phase, on the other hand, is formed by a rigid fcc lattice of S atoms where cations are randomly distributed over tetrahedral and octahedral interstitial sites.[8] This degree of disorder confers to these two HT phases important ion-transport properties, such as a high ionic conductivity.[8,9]

As seen above, the temperature effect on the stromeyerite structure has been extensively studied. The influence of the other critical thermodynamic variable, on the contrary, has not been studied so far. In this context, it is worth mentioning the renewed interest regarding the high-pressure (HP) phases of M_2S binary sulfides (where M is a monovalent metal) and, more particularly, their atomic arrangements.[10−15] Recent results evidence the existence of a common trend in pressure-induced transformations of alkaline-metal sulfides, which depends on coordinates of pressure and ionic radii ratio.[13] Therefore, the present work aims at studying experimentally the structural stability of AgCuS, a group IB MM′S sulfide, trying to understand its behavior under strong compression. The existing differences with other known binary sulfides will also be discussed. First-principles calculations have complemented the experimental measurements, giving support to and chemical insight into the observed behavior of silver−copper sulfide.

2. EXPERIMENTAL DETAILS

AgCuS was synthesized from a stoichiometric mixture of the binary sulfides.[4] Ag_2S (Sigma-Aldrich 99.9%) and Cu_2S (obtained by the reaction of the elements at 500 °C in an evacuated quartz ampule over 30 h) have been reacted at 300 °C in an evacuated glass ampule over 50 h. Powder X-ray diffraction (XRD) with Cu Kα radiation of the dark-gray metallic product identifies the stromeyerite and an impurity of 2.5% elemental silver as calculated by Rietveld refinement. The silver impurity occurs from a possible loss of copper and sulfur during the reaction (some red color was recognized on the wall of the ampule), but it can also approve the possible deficiency of Ag atoms in a defect structure.[4]

Two independent HP angle-dispersive XRD (ADXRD) experiments were conducted in diamond anvil cells at room temperature up to 13 GPa. Experiment 1 was carried out using an Xcalibur diffractometer with Mo Kα radiation (0.7107 Å). The AgCuS metallic-lustered powder sample was loaded in a 160-μm-diameter hole of a stainless steel gasket preindented to a thickness of about 50 μm. A 16:4:1 methanol/ethanol/water mixture was used as the pressure-transmitting medium. XRD patterns were obtained on a 135-mm Atlas charge-coupled detector (CCD). The X-ray beam could only be collimated to a diameter of 300 μm and, consequently, peaks of the stainless steel gasket appear above 2θ = 18.3°. Therefore, only the HP diffraction patterns below this angle were considered. The *CrysAlis* software was used for data collection and preliminary data reduction.

Experiment 2 was performed at the MSPD beamline of the ALBA synchrotron[16] with an incident monochromatic wavelength of 0.4246 Å. The sample loading was similar to that of experiment 1. The monochromatic X-ray beam was focused down to 50 × 50 μm. The images were collected using a SX165 CCD. Preliminary data reduction was done using the *Fit2D* software.[17] The pressure was measured by two different methods: (i) the ruby fluorescence scale[18] and (ii) the equation of state (EOS) of silver,[19] which is present as an impurity in our sample. Both methods give pressure values within 0.1 GPa in the whole pressure range of this study. The observed intensities were integrated as a function of 2θ in order to give conventional, one-dimensional diffraction profiles. The indexing and refinement of the powder XRD patterns were performed using the *FULLPROF*[20] and *POWDERCELL*[21] program packages. This second experiment provides high-quality data (more photons and a wider 2θ range) for unequivocal structure determination.

3. COMPUTATIONAL DETAILS

First-principles total-energy calculations were carried out within the density functional theory (DFT) formalism with a plane-wave pseudopotential approach, as implemented in the Vienna ab initio simulation package.[22] We used the projector-augmented-wave all-electron description of the electron ion−core interaction.[23] Brillouin-zone integrals were approximated using the method of Monkhorst and Pack.[24] The energies converged with respect to the *k*-point density (12×8×8 mesh for the orthorhombic $Cmc2_1$ RP structure and 8×8×4 mesh for the tetragonal $P4/nmm$ HP1 and monoclinic $P2_1n$ HP2 structures), and the plane-wave cutoff was kept fixed at a value of 420 eV. Initially, we used a conventional DFT exchange-correlation functional, within the generalized gradient approximation, the Perdew−Burke−Ernzerhof functional.[25]

However, transition-metal compounds such as AgCuS experience strong intraatomic exchange and Coulombic repulsion among the d electrons because of the many electrons and the localized, tight nature of the wave functions involved. Because DFT does not properly cancel out the electron self-interaction, the electron−electron repulsion is overestimated and, as a result, the electrons are incorrectly delocalized to reduce the repulsion energy. In short, the degree of covalence is overestimated. To overcome the failure of DFT to describe the strongly correlated "d" electrons of Ag and Cu, the rotationally invariant form of DFT+*U* was employed.[26] Within this approach, the Hubbard *U*, which is the Coulombic energetic cost to place two electrons at the same site, and the approximation of Hund's exchange parameter *J* can be grouped into the single effective parameter U_{eff}. It can be understood as the introduction of a penalty function, which disfavors noninteger occupation numbers of the on-site density matrix. It acts to reduce the one-electron potential locally for the Ag and Cu d orbitals, therefore reducing hybridization with orbitals of the S atoms. According with the literature, we have considered a U_{eff} = 5 eV for Ag[11] and Cu.[27,28]

All structural relaxations were performed via a conjugate-gradient minimization of the total energy using the tetrahedron method with Blochl corrections.[29] We note that the calculated enthalpy versus pressure [$H(p)$] curves correspond to the static approximation (zero temperature and neglecting zero-point vibrational contributions).

4. RESULTS AND DISCUSSION

The room-pressure (RP) XRD pattern, depicted in Figure 2, corresponds to the orthorhombic $Cmc2_1$ structure previously reported,[5] with similar lattice parameters and fractional atomic coordinates (see Table 1). Note the existence of a small amount (about 2.4 wt %) of metallic silver impurity (asterisk mark in Figure 2). In order to better understand the behavior of stromeyerite under compression, we should dwell on its atomic arrangement at ambient conditions. The structure is essentially based on a strong distortion of a Ni_2In-type structure (AuRbS-type). A projection of the structure is displayed in Figure 1. The planes parallel to (001) are composed of layers of loosely packed fcc Ag atoms (distances Ag−Ag ranging from 3.88 to 4.06 Å) alternating with graphite-like layers that can be considered as the interpenetration of two distorted S and Cu hexagonal packed nets. Consequently, the Cu and S atoms are triangularly coordinated, with distances 2 × 2.24 and 1 × 2.33 Å. These layers are arranged in such a way that the hexagonal 3^6 layers of S atoms (graphite-like 6^3 layers of S/Cu atoms) are bridged by two-coordinated Ag atoms (d_{Ag-S} = 1 × 2.42 and 1 × 2.44 Å). In fact, this bicoordination of Ag is caused by the distortion (compression) along the [0−11] direction of the octahedral sites of the S packing. The atomic arrangement resembles that of the Ni_2In-type structure, where the linear

dx.doi.org/10.1021/ic302116b | *Inorg. Chem.* 2013, 52, 355−361

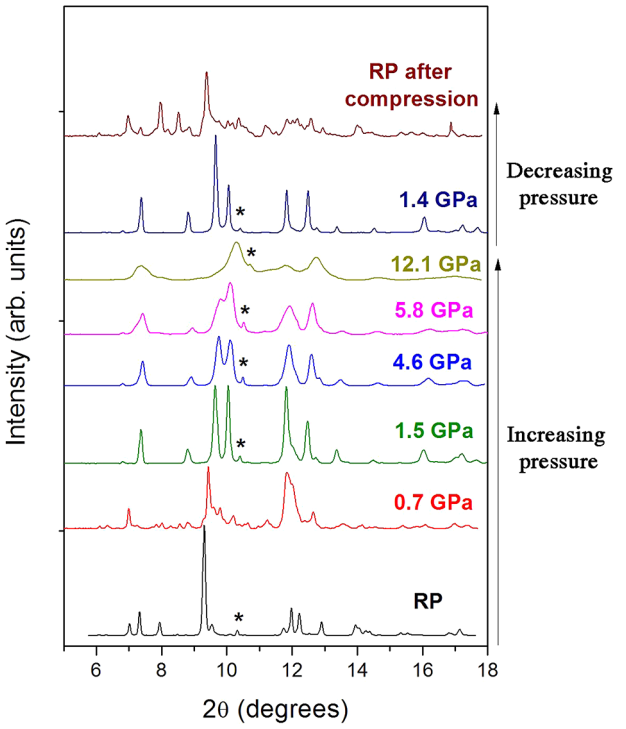

Figure 2. Powder XRD patterns of AgCuS at different pressure conditions. Upstroke and downstroke processes are indicated on the right-hand side. Asterisks denote the diffraction maxima of silver.

Table 1. Lattice Parameters and Fractional Coordinates of the RP Phase of Stromeyerite, AgCuS[a]

atom type	Wyckoff position	*x*	*y*	*z*
Ag	4a	0.5	0.4889(15)	0.4746(5)
Cu	4a	0	0.4294(2)	0.214(4)
S	4a	0.5	0.2910(2)	0.2195(5)

[a]Residuals in Rietveld refinements: R_P = 14.3; R_{WP} = 27.6. Space Group $Cmc2_1$ (No. 36), Z = 4, a = 4.06726(1) Å, b = 6.64064(4) Å, and c = 7.97111(2) Å.

chains of S-centered $[Ag_3Cu_3]$ trigonal prisms characteristic of this structural type are so close to each other that they almost overlap and, as a result, there exist very short Cu−Ag distances (2 × 2.84 and 2 × 2.93 Å). Thus, in this warped 4^4 Cu−Ag metallic layer, the interatomic distances are similar to those existing in elemental fcc silver and only slightly larger than those in elemental fcc copper (d_{Cu-Cu} = 2.56 Å), which suggests that metallic interaction may be important in this structure. This fact was already pointed out in a previous room- and low-temperature study on AgCuS stromeyerite.[5]

This phase starts to transform into a new HP structure at pressures below 0.7 GPa. The XRD pattern at this pressure was completely different from that at ambient conditions and could not be unequivocally indexed. The large amount of Bragg peaks in this pattern suggests that one or several polymorphs with intermediate structures could coexist. No experimental EOS of the RP phase could be obtained, but first-principles DFT calculations suggest a third-order Birch−Murnaghan EOS with parameters V_0 = 233.04 Å^3, B_0 = 26.46, and B'_0 = 4.48. At 1.5 GPa, however, the XRD pattern presents only 14 well-defined maxima, which were indexed into a tetragonal space group with the lattice parameters a = 3.91188(2) Å and c = 18.5474(2) Å, with a good figure of merit. The $h + k = 2n$ reflection condition in the indexed ($hk0$) lattice planes is consistent with an *n*-glide plane normal to the *c* axis, which suggests either *P*4/*nmm* or *P*4/*n* symmetry. At this point, it is important to point out that AgCuSe was initially reported to have a tetragonal structure[30] and space group *P*4/*nmm* with lattice constants $a \sim 4.09$ Å and c = 6.31 Å (Z = 2) and later found to have an orthorhombic superstructure[31] based on this tetragonal subcell. Interestingly, the structural model of AgCuSe (anti-PbClF-type) is valid for AgCuS considering that the *klassengleiche* subgroup relationship allows trebling the length of the *c* axis. An XRD pattern of this phase is shown in Figure 3 to illustrate the quality of the

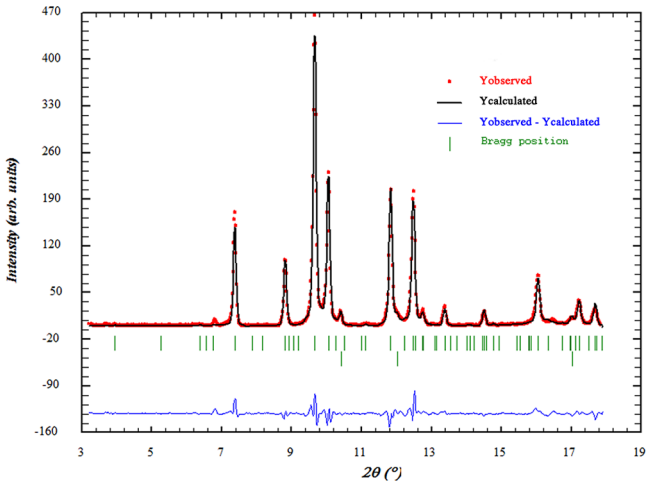

Figure 3. Rietveld refinement of the XRD pattern at 1.4 GPa on downstroke. Observed, calculated, and difference XRD profiles are represented as red, black, and blue lines, respectively. Vertical marks indicate the Bragg reflections of the tetragonal *P*4/*nmm* AgCuS structure (top) and metallic silver (bottom).

Rietveld refinement. The refined parameters were as follows: the overall scale factor, the cell parameters, the pseudo-Voigt profile function with terms to account for the reflection anisotropic broadening, the fractional atomic coordinates, and the background. The atomic positions of this HP phase are collected in Table 2. It should also be stressed that the tetragonal subcell with *c*/3 would explain the position and intensity of 13 of the 14 Bragg peaks of the diffractogram.

This HP1 phase (see Figure 4) can be properly described as follows: As said above, it crystallizes as tetragonal crystals (space group *P*4/*nmm*) with the PbFCl-type structure, having a

Table 2. Lattice Parameters and Fractional Coordinates of the HP1 Phase of AgCuS at 1.4 GPa[a]

atom type	Wyckoff position	*x*	*y*	*z*
Ag1	2c	0.25	0.25	0.4545(7)/**0.45022**
Ag2	2c	0.25	0.25	0.7862(7)/**0.78362**
Ag3	2c	0.25	0.25	0.1146(9)/**0.11692**
Cu1	2a	0.75	0.25	0/**0**
Cu2	4f	0.75	0.25	0.3288(12)/**0.3333**
S1	2c	0.25	0.25	0.601(2)/**0.59039**
S2	2c	0.25	0.25	0.918(2)/**0.92379**
S3	2c	0.25	0.25	0.233(3)/**0.25709**

[a]Residuals in Rietveld refinements: R_P = 12.3; R_{WP} = 20.5. In bold, theoretically calculated atomic coordinates based on the tetragonal subcell with *c*/3, reported in Table 4. Space group *P*4/*nmm* (No. 129), Z = 6, a = 3.90312(15) Å, and c = 18.5268(14) Å.

dx.doi.org/10.1021/ic302116b | *Inorg. Chem.* 2013, 52, 355−361

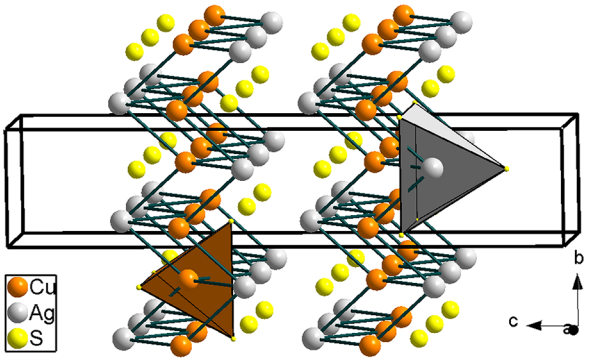

Figure 4. Structure of the HP1 phase of AgCuS.

supercell 3 times larger ($c' = 3c$) than other MM′S sulfides like Li(Na,K,Rb)S or Na(Rb,Cs)S at ambient pressure. In this phase (at 1.5 GPa), Cu is tetrahedrally surrounded by four S atoms (Cu−S = 1 × 2.38 and 3 × 2.44 Å) to form $^{2}_{\infty}[Cu^{[2;\,4]}S]$ layers perpendicular to the c axis; i.e., each $[CuO_4]$ tetrahedron shares four edges with four neighboring tetrahedra (see ref. 32 for nomenclature support). Silver, on the other hand, is five-coordinated and forms $[AgS_5]$ square pyramids (average d_{Ag-S} = 1 apical × 2.5 and 4 base × 2.87 Å), which are placed between the [CuS] layers. Thus, compared with the RP phase, the coordination number of Cu by S atoms increases from 3 to 4, whereas that of the Ag atoms decreases from 6 (2 + 4) to 5. The S anion sublattice, however, is still formed by hexagonal layers. Note that this structure also exhibits very short Cu−Cu (4 × 2.74 Å in planar 4^4-layered configuration) and Cu−Ag distances (3 × 2.88 and 1 × 3.03 Å), which grant metallic properties to this HP phase. These metal−metal distances are compared to those of the RP phase (see Table 3), which, in turn, are comparable to those of the metallic elements.

Table 3. Metal−Metal Bond Lengths (Å) in the $Cmc2_1$ RP Phase and the P4/*nmm* HP1 Phase at 1.4 GPa[a]

	RP (space group $Cmc2_1$)	HP1 (space group $P4/nmm$)
Cu−Cu	4 × 3.89	4 × 2.74
	2 × 4.07	4 × 3.90
	2 × 4.09	
Cu−Ag	2 × 2.84	
	2 × 2.93	3 × 2.88
	1 × 3.37	1 × 3.03
	1 × 3.59	
Ag−Ag	4 × 3.88	4 × 3.37
	2 × 3.98	4 × 3.90
	2 × 4.06	

[a]Only distances below 4.2 Å are collected in the table.

The compressibility of this HP phase has been estimated by fitting a third-order Birch−Murnaghan EOS to our pressure−volume data (Figure 5a). The following values for the zero-pressure volume and the bulk modulus were obtained by fixing the pressure derivative B'_0 to 4: V_0 = 287.9(2) Å^3; B_0 = 104(3) GPa. The compression of the lattice parameters is slightly anisotropic; i.e., relative contractions between 1.5 and 3.5 GPa are 0.72% and 0.32% for the a and c axes, respectively (see Figure 5b). From this pressure, the c axis remains almost incompressible and the a axis contracts more rapidly, with the volume decreasing in a continuous manner, as seen in Figure 5a. The incompressibility of the larger axis above 3.5 GPa is

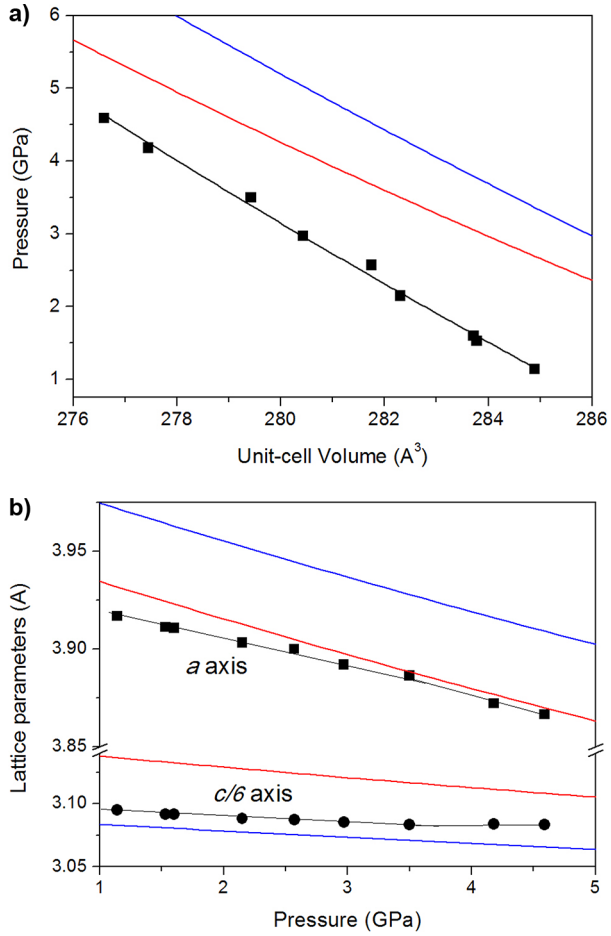

Figure 5. (a) Experimental and calculated pressure dependences of the unit-cell volume for the HP1 phase of AgCuS. Black squares correspond to the experimental data, whereas the solid blue and red lines correspond to DFT and DFT+U calculations. (b) Evolution of the lattice parameters of the HP1 phase with pressure. Squares and circles represent the a and $c/6$ axes.

likely related to strong Ag−Ag repulsions between 4^4 Cu−Ag layers.

Above 4.6 GPa, the diffraction peaks broaden significantly. Note that the mixture MeOH/EtOH/H_2O used as the pressure medium assures quasi-hydrostatic conditions up to 10.5 GPa[33] and, therefore, the peak broadening cannot be explained by deviatoric stresses. This seems to be the onset of another phase transition. The few changes observed in the intensities of the Bragg peaks suggest this HP2 phase to be a distortion of the HP1 one. A monoclinic structure, described in the $P2_1/m$ subgroup of the $P4/nmm$ structure, would explain the observed peak broadening. Thus, a tentative unit cell of a = 3.868(2) Å, b = 3.848(2) Å, c = 18.515(6) Å, and β = 91.83(3)° is proposed at 5.7 GPa. This second phase transition will be further discussed below. No experimental EOS could be obtained. In the decompression process, the HP2 phase transforms into HP1, which presents again sharp Bragg peaks. After pressure release, the initial orthorhombic $Cmc2_1$ phase was not recovered (see Figure 2).

Our experimental observations are supported by ab initio total-energy calculations. As mentioned in the Computational Details section, two independent sets of data were calculated using the DFT and DFT+U approximations. As can be seen in Figure 6, the theoretical DFT+U energy−volume curves of the

dx.doi.org/10.1021/ic302116b | Inorg. Chem. 2013, 52, 355−361

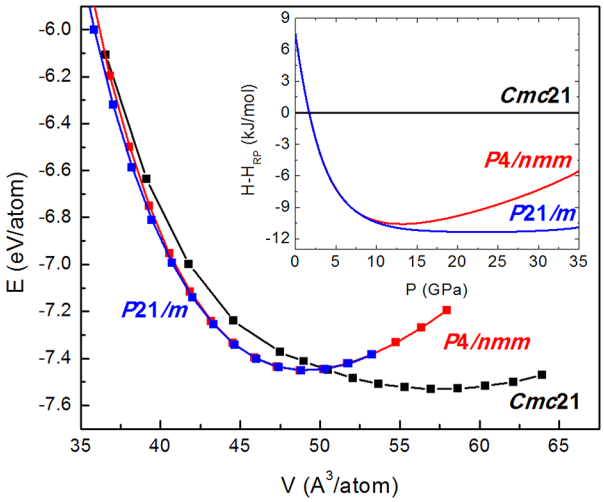

Figure 6. Cohesive energy as a function of the volume for the initial $Cmc2_1$, the HP1 $P4/nmm$, and the HP2 $P2_1/m$ structures of AgCuS. Inset: Enthalpy variation versus pressure.

initial RP and HP1 phases cross each other at HP (at 2.6 GPa, inset of Figure 6). Note that in the calculations we have used the tetragonal subcell in which the experimental indexed lattice is based, whose c dimension is a third of that one ($Z = 2$). The tetragonal HP1−monoclinic HP2 phase transition is theoretically predicted at 6.1 GPa. On the other hand, using the DFT approach, only one phase transition to HP2 at 5.3 GPa is observed. A phase diagram more consistent with the experimental data can therefore be obtained under the DFT +U approach. The range of stability of the $P4/nmm$ HP1 phase is consistent with experiments with a value $U_{eff} = 5$, showing the importance of the inclusion of correlation effects.

As can be seen in Table 2, the calculated fractional coordinates of HP1 compare very well to those from our experiment, but the lattice parameter c and the unit-cell volume are significantly overestimated (>0.56% in volume; Figure 5 and Table 4). The calculated compressibility using DFT is in

Table 4. Theoretical DFT+U Lattice Parameters and Fractional Coordinates of the HP1 Phase of AgCuS at 1.4 GPa[a]

atom type	Wyckoff position	x	y	z
Ag	2c	0.25	0.25	0.35075
Cu	2a	0.75	0.25	0
S	2c	0.25	0.25	0.77128

[a]Space group $P4/nmm$ (No. 129), $Z = 2$, $a = 3.89595$ Å, and $c = 6.23374$ Å.

better agreement with that estimated experimentally than using the DFT+U approach, as can be deduced from looking at the theoretical and experimental evolution of the lattice volumes with pressure in Figure 5a. Thus, for the subcell with two formula units per cell, the following characteristic parameters were obtained: $V_0 = 98.41$ Å^3, $B_0 = 80$ GPa, and $B'_0 = 5.26$ ($V_0 = 98.4$ Å^3 and $B_0 = 89$ GPa if B'_0 is fixed to 4 to be better compared with the experimental data) and $V_0 = 98.25$ Å^3, $B_0 = 73$ GPa, and $B'_0 = 5.17$ for DFT and DFT+U, respectively. It is important to mention that the RP−HP1 transformation entails a volume decrease of 9.7%.

Theoretical calculations also predict that the tetragonal phase starts to distort to a monoclinic phase at 6.1 GPa. See, for instance, the calculated lattice parameters and fractional coordinates of the HP2 phase at 8.6 GPa in Table 5. The

Table 5. Theoretical DFT+U Lattice Parameters and Fractional Coordinates of the HP2 Phase of AgCuS at 8.6 GPa[a]

atom type	Wyckoff position	x	y	z
Ag	2e	0.72582	0.25	0.64979
Cu	2e	0.25354	0.25	0.99973
S	2e	0.76724	0.25	0.23257

[a]Space group $P2_1/m$ (No. 11), $Z = 2$, $a = 3.8113$ Å, $b = 3.8122$ Å, $c = 6.15039$ Å, and $\beta = 92.085°$.

evolution of the lattice constants of this phase is depicted in Figure 7. As can be seen, the β angle rapidly increases with

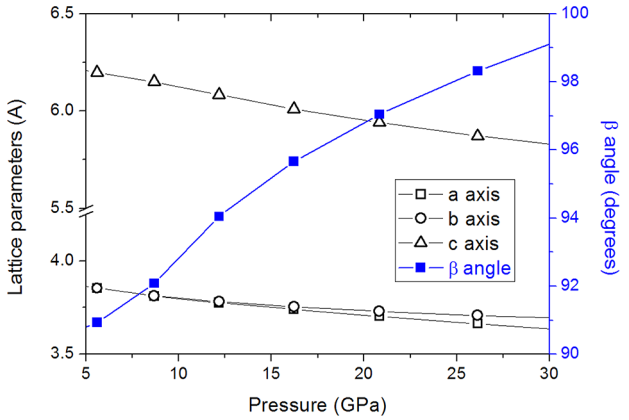

Figure 7. Evolution of the lattice constants and the β angle of the theoretically predicted HP2 phase (space group $P2_1/m$).

pressure (at 32.3 GPa, $\beta = 99.57°$). Regarding its compressibility, it does not differ much from that of the tetragonal HP1 phase. No volume discontinuity occurs at this phase transition, suggesting a displacive second-order transition.

To our best knowledge, the structural sequence of stromeyerite AgCuS under compression has never been experimentally observed in other compounds. The AuRbS-type (distorted Ni_2In-type) structure stable at room conditions transforms into an anti-PbClF-type structure (HP1) at HP. This transition entails a complete rearrangement of atoms, although the four-connected CuS subarray is still recognizable (see Figure 8). When both structures are compared, it is advisable that the main difference resides in the location of the Ag atoms. Thus, in the tetragonal HP1 phase of AgCuS, the Ag atoms are coplanar (parallel to the bc plane) with the Cu and S atoms, in contrast with that occurring in the $Cmc2_1$ RP phase. It is also remarkable that the CuS subarray in the HP1 phase coincides with the structure of FeS. This can be explained in light of the Zintl−Klemm concept, assuming that the Ag atoms transfer their valence electrons to the CuS framework, forming a $[CuS]^-$ polyanion that is isoelectronic with FeS. Once more, this single theoretical concept gives a consistent overview of the structural behavior of an inorganic compound.[34−36]

Most of the MM′S alkaline-metal mixed sulfides (M and M′ = Li−Cs) adopt the tetragonal $P4/nmm$ HP1 structure at ambient conditions. Two exceptions are NaKS and RbKS, which are anti-$PbCl_2$-like structures. The tetragonal structure of the HP1 phase is not found, however, for any binary M_2S

dx.doi.org/10.1021/ic302116b | Inorg. Chem. 2013, 52, 355−361

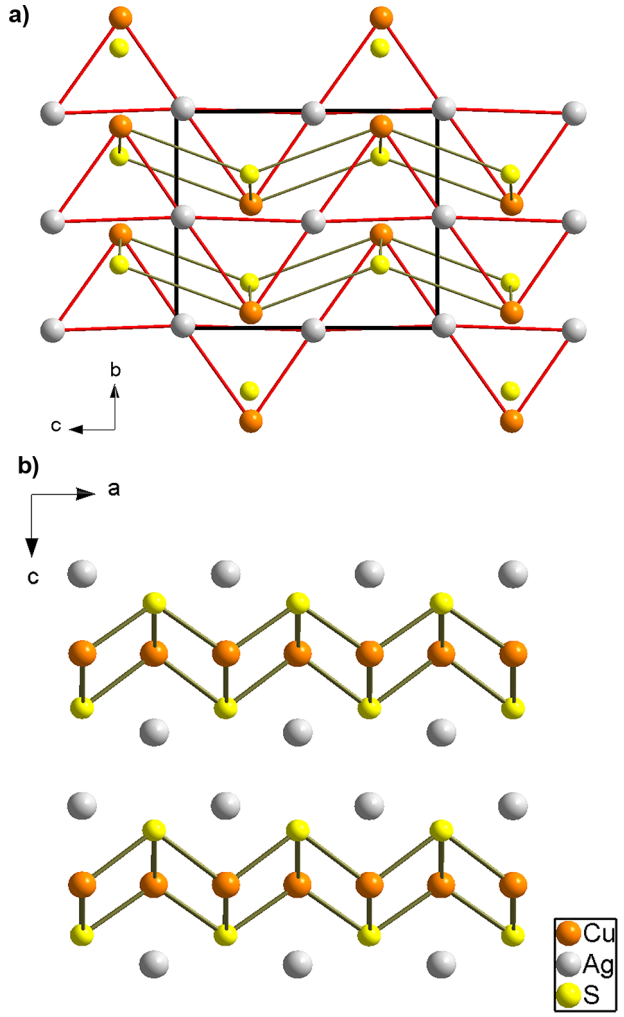

Figure 8. (a) Distorted Ni_2In-type structure of AgCuS at RP showing the underlying four-connected CuS subarray. A strong distortion of this 4^4 subnet is present in the tetragonal HP1 phase (b).

alkaline−metal sulfide. Consequently, one could think that MM′S mixed sulfides with two metals of different atomic radii will tend to produce such a structure. Moreover, as we have seen, this only occurs in AgCuS at HPs (above 1 GPa), showing that the group IB sulfides present distinguishing features. Up to now, no HP studies existed on this class of compounds; that is why this work paves the way for the understanding of their structural phase transitions. It is expected that copper, silver, and gold mixed sulfides have a different structural behavior under compression related to the larger electronegativity values of these metals, in comparison to alkaline metals. Further studies are needed to confirm such a hypothesis because it could also occur that chemical bonds in alkaline-metal and transition-metal sulfides become closer in covalent character under compression.

5. CONCLUDING REMARKS

The structural stability of stromeyerite, AgCuS, has been studied both experimentally and theoretically. ADXRD measurements up to 13 GPa show two phase transitions at 1.4 and 5.7 GPa, respectively. The first pressure-induced transition is from a distorted Ni_2In-type (RP, space group $Cmc2_1$) to an anti-PbClF-type structure (HP1, space group $P4/nmm$), which is very common among the MM′S alkaline-metal mixed sulfides at ambient conditions. In the initial orthorhombic phase, Ag−Cu interatomic distances are close to those existing in elemental fcc silver and only slightly larger than those in elemental fcc copper, which suggests that metallic interaction may be important. The tetragonal HP1 phase presents very short Ag−Cu distances as well, but the Cu−Cu and Ag−Ag distances are also comparable with those of the corresponding metallic elements (see Table 3), likely stressing the metallic properties of this HP phase. Moreover, a second phase transition to a monoclinic distortion (space group $P2_1/m$) of the tetragonal phase has been suggested. Finally, the initial orthorhombic RP phase was not recovered after decompression. Ab initio total-energy calculations complement the experimental results and confirm the HP phase sequence.

AUTHOR INFORMATION

Corresponding Author

*E-mail: dsantamaria@quim.ucm.es.

Notes

The authors declare no competing financial interest.

‡MALTA Consolider Team.

ACKNOWLEDGMENTS

Financial support from the Spanish Consolider Ingenio 2010 Program (Project CDS2007-00045) is acknowledged. The work was also supported by Spanish MICCIN under Projects CTQ2009-14596-C02-01 and MAT2010-21270-C04-01, as well as by Comunidad de Madrid and European Social Fund S2009/PPQ-1551 4161893 (QUIMAPRES). The ALBA Synchrotron Light Source is acknowledged for the provision of beamtime. We thank Drs. Peral, Popescu, and Fauth for technical support and constructive discussions. A.M.-G. and B.G.-D. are also grateful to the Spanish MICCIN for predoctoral fellowships.

REFERENCES

(1) Guild, F. N. *Econ. Geol.* **1917**, *12*, 297.
(2) Schwartz, G. M. *Econ. Geol.* **1935**, *30*, 128.
(3) Suhr, N. *Econ. Geol.* **1955**, *50*, 347.
(4) Frueh, A. J. *Z. Kristallogr.* **1955**, *106*, 299.
(5) Baker, C. L.; Lincoln, F. J.; Johnson, A. W. S. *Acta Crystallogr., Sect. B* **1991**, *47*, 891.
(6) Djurle, S. *Acta Chem. Scand.* **1958**, *12*, 1427.
(7) Skinner, B. J. *Econ. Geol.* **1966**, *61*, 1.
(8) Trots, D. M.; Senyshyn, A.; Mikhailova, D. A.; Knapp, M.; Baehtz, C.; Hoelzel, M.; Fuess, H. *J. Phys.: Condens. Matter* **2007**, *19*, 136204.
(9) Skomorokhov, A. N.; Trots, D. M.; Ovchinnikov, S. G.; Fuess, H. *J. Phys.: Condens. Matter* **2007**, *19*, 186228.
(10) Grzechnik, A.; Vegas, A.; Syassen, K.; Loa, I.; Hanfland, M.; Jansen, M. *J. Solid State Chem.* **2000**, *154*, 603.
(11) Santamaria-Perez, D.; Marques, M.; Chulia-Jordan, R.; Menendez, J. M.; Gomis, O.; Ruiz-Fuertes, J.; Sans, J. A.; Errandonea, D.; Recio, J. M. *Inorg. Chem.* **2012**, *51*, 5289.
(12) Santamaria-Perez, D.; Vegas, A.; Muehle, C.; Jansen, M. *Acta Crystallogr., Sect. B* **2011**, *B67*, 109.
(13) Santamaria-Perez, D.; Vegas, A.; Muehle, C.; Jansen, M. *J. Chem. Phys.* **2011**, *135*, 054511.
(14) Vegas, A.; Grzechnik, A.; Hanfland, M.; Muhle, C.; Jansen, M. *Solid State Sci.* **2002**, *4*, 1077.
(15) Vegas, A.; Grzechnik, A.; Syassen, K.; Loa, I.; Hanfland, M.; Jansen, M. *Acta Crystallogr., Sect. B* **2001**, *57*, 151.
(16) Knapp, M.; Peral, I.; Nikitina, M.; Quispe, M.; Ferrer, S. *Z. Kristallogr. Proc.* **2011**, *1*, 137.

(17) Hammersley, A. P.; Svensson, S. O.; Hanfland, M.; Fitch, A. N.; Hausermann, D. *High Press. Res.* **1996**, *14*, 235.
(18) Mao, H. K.; Xu, J.; Bell, P. M. *J. Geophys. Res., [Solid Earth Planets]* **1986**, *91*, 4673.
(19) Akahama, Y.; Kawamura, H.; Singh, A. K. *J. Appl. Phys.* **2004**, *95*, 4767.
(20) Rodriguez-Carvajal, J. *Physica B* **1993**, *192*, 55.
(21) Nolze, G.; Kraus, W. *Powder Diffr.* **1998**, *13*, 256.
(22) Kresse, G.; Furthmuller, J. *Phys. Rev. B* **1996**, *54*, 11169.
(23) Kresse, G.; Joubert, D. *Phys. Rev. B* **1999**, *59*, 1758.
(24) Monkhorst, H. J.; Pack, J. D. *Phys. Rev. B* **1976**, *13*, 5188.
(25) Perdew, J. P.; Burke, K.; Ernzerhof, M. *Phys. Rev. Lett.* **1996**, *77*, 3865.
(26) Dudarev, S. L.; Botton, G. A.; Savrasov, S. Y.; Humphreys, C. J.; Sutton, A. P. *Phys. Rev. B* **1998**, *57*, 1505.
(27) Arroyo y de Dompablo, M. E.; Lee, Y. L.; Morgan, D. *Chem. Mater.* **2010**, *22*, 906.
(28) Lei, W.; Maxisch, T.; Ceder, G. *Phys. Rev. B* **2006**, *73*, 195107.
(29) Blochl, P. E. *Phys. Rev. B* **1994**, *50*, 17953.
(30) Earley, J. W. *Am. Mineral.* **1950**, *35*, 337.
(31) Frueh, A. J.; Czamanke, G. K.; C.H., , K. *Z. Kristallogr.* **1957**, *108*, 389.
(32) Santamaria-Perez, D.; Vegas, A.; Liebau, F. *Struct. Bonding (Berlin)* **2005**, *118*, 121.
(33) Klotz, S.; Chervin, J. C.; Munsch, P.; Le Marchand, G. *J. Phys. D* **2009**, *42*, 7.
(34) Santamaria-Perez, D.; Vegas, A. *Acta Crystallogr., Sect. B* **2003**, *59*, 305.
(35) Santamaria-Perez, D.; Liebau, F. *Struct. Bonding (Berlin)* **2011**, *138*, 1.
(36) Vegas, A. *Struct. Bonding (Berlin)* **2011**, *138*, 133.